4-14-2015

Structural insights into the cubic-hexagonal phase transition kinetics of monoolein modulated by sucrose solutions

Caleb W. Reese
Calvin University

Zachariah I. Strango
Calvin University

Zachary R. Dell
Carnegie Mellon University

Stephanie Tristram-Nagle
Carnegie Mellon University

PCCP

PAPER

View Article Online
View Journal | View Issue

Cite this: *Phys. Chem. Chem. Phys.*, 2015, **17**, 9194

Structural insights into the cubic–hexagonal phase transition kinetics of monoolein modulated by sucrose solutions

Caleb W. Reese,[a] Zachariah I. Strango,[a] Zachary R. Dell,[b] Stephanie Tristram-Nagle[b] and Paul E. Harper*[a]

Received 12th January 2015,
Accepted 3rd March 2015

DOI: 10.1039/c5cp00175g

www.rsc.org/pccp

Using DSC (differential scanning calorimetry), we measure the kinetics of the cubic–H_{II} phase transition of monoolein in bulk sucrose solutions. We find that the transition temperature is dramatically lowered, with each 1 mol kg^{-1} of sucrose concentration dropping the transition by 20 °C. The kinetics of this transition also slow greatly with increasing sucrose concentration. For low sucrose concentrations, the kinetics are asymmetric, with the cooling (H_{II}–cubic) transition taking twice as long as the heating (cubic–H_{II}) transition. This asymmetry in transition times is reduced for higher sucrose concentrations. The cooling transition exhibits Avrami exponents in the range of 2 to 2.5 and the heating transition shows Avrami exponents ranging from 1 to 3. A classical Avrami interpretation would be that these processes occur *via* a one or two dimensional pathway with variable nucleation rates. A non-classical perspective would suggest that these exponents reflect the time dependence of pore formation (cooling) and destruction (heating). New density measurements of monoolein show that the currently accepted value is about 5% too low; this has substantial implications for electron density modeling. Structural calculations indicate that the head group area and lipid length in the cubic–H_{II} transition shrink by about 12% and 4% respectively; this reduction is practically the same as that seen in a lipid with a very different molecular structure (*rac*-di-12:0 β-GlcDAG) that makes the same transition. Thermodynamic considerations suggest there is a hydration shell about one water molecule thick in front of the lipid head groups in both the cubic and H_{II} phases.

1 Introduction

Monoolein is a deceptively simple lipid that exhibits a rich array of temperature and composition sensitive behavior. Lamellar, inverted hexagonal, sponge phases and minimal surface based cubic phases are all part of monoolein's extensive and intriguing structural repertoire.[1,2] When one considers that it is inexpensive, biodegradable and so non-toxic as to be commonly used a food additive, the range of possible applications becomes immense. Monoolein and similar lipids are used as drug delivery systems, as matrices for membrane protein crystallization and even as templates for the creation of 3-D metal nanowire networks. The fascinating phase behavior and numerous applications have led to the thousands of papers and patents that study or utilize monoolein; consequently, this has led some to describe monoolein as a 'magic lipid'.[3,4]

In excess water, monoolein forms a minimal surface based phase (see Fig. 1) over a broad temperature range running from below room temperature to 90 °C. The minimal surface in this case is known as the D surface; it has cubic unit cell and can be

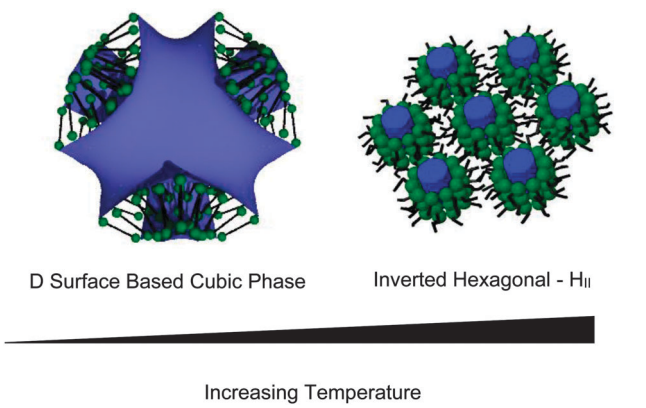

Fig. 1 Depictions of lipid phases. Lipid heads are shown as green spheres and the tails as black lines. Bluish-purple surfaces mark the lipid–water interface in the D surface based cubic phase; blue cylinders in the H_{II} phase indicate the water cores.

[a] *Department of Physics and Astronomy, Calvin College, 1734 Knollcrest Circle SE, Grand Rapids, MI, USA. E-mail: pharper@calvin.edu; Fax: +1 616 526 6501; Tel: +1 616 526 6408*

[b] *Biological Physics Group, Physics Department, Carnegie Mellon University, 5000 Forbes Avenue, Pittsburgh, PA 15213, USA*

stacked three dimensionally. A lipid bilayer straddles the minimal surface and divides space into two identical but separate water channel networks. There are several minimal surface based phases with cubic unit cells. For simplicity's sake, we will use cubic to refer to the D surface based phase in this paper. In depth dimensional and phase data can be found in Briggs *et al.*[1] and Qiu and Caffrey;[2] further information on minimal surfaces in general and electron density modeling and reconstruction of monoolein in particular are found in Harper and Gruner[5] and Harper *et al.*[6] Above 90 °C, monoolein transitions to the inverted hexagonal (H_{II}) phase, which consists of water cylinders wrapped in lipid monolayers which are in turn stacked in a hexagonal pattern (see Fig. 1).

In depth structural studies have been performed on phosopholipids that form the H_{II} phase[7–9] and monoolein itself in this phase has recently been the focus of molecular dynamics simulation.[10]

The non-lamellar structures seen in monoolein are seen not only in a variety of lipid systems, including lipids with PE (phosphatidylethanolamine) headgroups[7,11] and PC (phosphatidylcholine) headgroups,[12] but also in block copolymers.[13,14] Non-lamellar phase behavior offers a deep window into fundamental processes such as membrane fusion.[15–17] Furthermore, non-lamellar phase behavior has been useful in understanding the action of anti-microbial peptides.[18–21] Several other examples of biological relevance can be found in Cook *et al.*[22] Given the ubiquity, beauty and biological relevance of these phases, there has been considerable theoretical interest[23–27] and this remains an active area of inquiry.

The cubic phase in monoolein is especially attractive for encapsulating drugs as it is stable both at room and physiological temperatures. It is quite viscous, allowing for the deposition of stable thin films. Since the cubic phase is a lipid–water matrix, both hydrophobic and hydrophilic drugs can be incorporated.[28,29] A wide variety of drug release systems have been developed, including a tunable, pH dependent matrix[30] and a magnetic field controlled system in which ferromagnetic nanoparticles are incorporated into the matrix.[31]

Another important application of monoolein is in the field of membrane protein crystallization.[32,33] The cubic phases enable the formation of crystals in which the proteins are embedded in a lipid bilayer, a configuration much closer to the native state. It has long been known that membrane properties and composition deeply affect membrane protein function.[34] Consequently, lipid–protein crystals offer a fruitful arena for examining the effects of membrane composition on proteins.[35–37] There are also promising efforts to use these crystals to probe femtosecond time scale behavior of proteins.[38]

Given the rich array of structures formed by monoolein and the wealth of applications, there are a number of studies considering the effects of various additives.[39–41] There also have been extensive investigations of cosmotropic and chaotropic solutes, especially sugars, on the fluid lamellar L_α to H_{II} transition (see Koynova *et al.*[42] and references therein). Sugar–lipid interactions are particularly noteworthy as sugars are often used by living systems to stabilize their membranes; the detailed mechanism by which this occurs is an ongoing area of investigation.[43] Surprisingly, there has been a relative dearth of work on sugar–monoolein mixtures, with most investigations focused on structure studies of isothermal mixtures.[44–47] Our work starts to fill that gap by mapping out the phase diagram of monoolein with an excess of sucrose–water solutions at a variety of concentrations.

Phase transition kinetic studies and their analysis are challenging, but potentially quite rewarding. Phase transitions often involve the rupture and repair of membranes; hence, understanding the kinetics could ultimately reveal information about pore formation energetics and time scales. Often performed at X-ray synchrotrons, there have been several studies on cubic kinetics[48–50] and some theoretical effort as well.[51] We probe the kinetics of the cubic–H_{II} phase transition in monoolein–sucrose–water mixtures using DSC (differential scanning calorimetry). Avrami theory, a powerful tool for phase transition analysis,[52] has been brought to bear on lipid phases transitions involving lamellar phases[53] and for the L_α–H_{II} transition.[22] In this work, we apply Avrami theory to a cubic–H_{II} transition for the first time.

2 Materials and methods

Monoolein was obtained from Nu Check Prep (Elysian, MN) in powder form with a purity >99% and sucrose was procured from Sigma Aldrich (St. Louis, MO) in polycrystalline form with a purity ≥99.5%.

2.1 Density measurements

The concentration of monoolein samples varied from 0.5–5 wt%, with the most successful samples prepared at <1 wt%. Monoolein powder (~10 mg) and milliQ water (~1.2 g) were weighed on an analytical balance (Mettler AE 163). The sample was heated in an oven at 60 °C for 10 minutes and sonicated briefly, 3 times 3 s. bursts, at room temperature. The sample was replaced at 60 °C for 10 minutes, resonicated in short bursts, replaced at 60 °C for 30 minutes and resonicated in short bursts. Care was taken not to cause foam on the top of the sample from the sonication. This sample preparation differed from the usual protocol of temperature cycling between 60 °C and −20 °C with vortexing,[54] since vortexing and cold temperature caused the lipid to clump. Samples with a monoolein concentration >1 wt% also clumped more easily. The sample was then loaded into the DMA 5000M densimeter (Anton-Paar) and held at 50 °C for three days prior to the first cooling scan. Six heating and cooling scans between 7 °C and 50 °C were performed with the density recorded at 0.5 °C increments. The heating scans occurred at a rate of 12 °C h^{-1} and the cooling scans at 4 °C h^{-1}. Data were averaged using the Origin 8 software and the standard deviation was calculated.

2.2 DSC measurements

DSC (differential scanning calorimetry) measurements were made using a TA Instruments (New Castle, DE) Q20 differential

scanning calorimeter. Stock solutions of sucrose were prepared, with concentrations ranging from 0.5 to 3.0 molality in 0.5 molality increments and sonicated for at least 20 minutes to ensure mixing. Samples were made by using a 10 μL Drummond dispenser (Broomall, PA) to transfer about 1 mg of monoolein and about 10 mg of sucrose solution to a Tzero hermetic pan (TA Instruments). The pan was then covered with a Tzero hermetic lid and sealed using a Tzero press. A sealed sample pan in which a small hole was made in the lid was used as a reference pan, as is the recommended practice with this instrument. DSC runs consisted of multiple heating and cooling scans at rates of 0.2, 0.1, 0.05, 0.02, and 0.01 °C s^{-1} over a range of temperatures that varied with the sucrose concentration and were in the region of about 20 °C to 90 °C. The sealed samples were weighed before and after the DSC measurements to check for leakage. If there was a deviation of more than a few hundredths of a mg between the weights, the sample was considered compromised and the data was not used. We found that under the repeated cycling, the likelihood of leakage strongly increased as temperatures neared 100 °C. The temperature of the cubic–H_{II} phase transition for monoolein and pure water is 90 °C;[1,2] at the elevated temperatures necessary to measure the kinetics of this transition, we inevitably encountered sample leakage and so were unable to measure the kinetics for monoolein and pure water.

3 Results and discussion

3.1 Density measurements – experimental results

The volume of monoolein as a function of temperature is shown in Fig. 2.

The sample in that figure was scanned repeatedly, heating and cooling, for a total of six scans. In addition, four partial scans were carried out, confirming the full scans. Between each heating and cooling scan the sample was removed and replaced in the densimeter, since we previously determined that lipid settling over time can cause an artifactual increase in density in the DMA densimeter.[54] The change of slope at 24 °C was quite reproducible. According to multiple phase diagrams of monoolein in water, there is no lipid phase transition near 24 °C at high hydration, such as in our sample.[1,2,57–59] According to these phase diagrams, monoolein is in the *Pn*3*m* cubic phase plus excess water both below and above 24 °C. Therefore, the origin of this transition is not known.

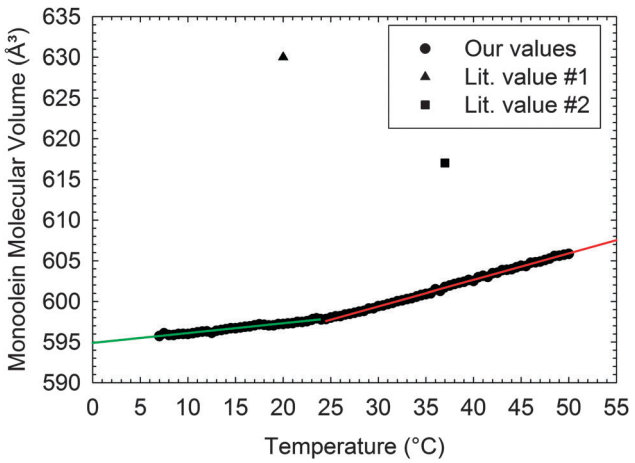

Fig. 2 Volume of monoolein as function of temperature; our data is plotted as filled circles and the uncertainties are comparable to the symbol size. The most common value cited for monoolein, Lit. value #1, is plotted as a filled triangle.[3,55] The other value found in the literature, Lit. value #2, is plotted as a filled square.[56] The data was well fit by two straight lines shown on the diagram, a green line for the region below 24 °C and and a red line for the region above. For temperatures less than 24 °C, the volume was well fit by V = (0.121 Å^3 °C^{-1})T + 594.9 Å^3. For temperatures above 24 °C, the volume was given by V = (0.326 Å^3 °C^{-1})T + 589.6 Å^3. In both formulas, V is the volume of monoolein and T is temperature.

3.2 Density measurements – comparison with literature

As seen in Fig. 2, the two values for the density of monoolein are at substantial odds with our results; consequently, it seems worthwhile to briefly review those literature values and note facts that support our results. Perhaps the most common value cited for the density of monoolein is 0.94 g cm^{-3} (molecular volume of 630 Å^3) at 20 °C.[3] The source for this value has been given as Sigma Aldrich[55] and as the CRC (Chemical Rubber Company) handbook,[6] with both sources giving the same value. As the CRC value for monoolein has been listed for at least 40 years, it is the likely the source used by Sigma Aldrich. A more recent measurement yielded 0.96 g cm^{-3} (617 Å^3) at 37 °C;[56] in that work, no mention of the other literature value was made. That measurement used a DMA 60 and a DMA 602 densitometer (Anton-Paar), which are both older, less accurate predecessors of the instrument used in this work. There are no explicit experimental accounts of whether or not the monoolein was hydrated in either of the measurements in the literature and so it is unknown as to the role hydration plays in the difference in densities. Nonetheless, it is noted that the higher temperature measurement has a higher density which does not seem likely.

In order to evaluate these densities, it is useful to consider the volumes and corresponding electron densities of monoolein's components. At 25 °C, the terminal methyl occupies 56 Å^3 and the remainder of the tail (excluding the carbon double bonded to the oxygen) occupies 413 Å^3. Using the old CRC handbook value for the density and applying a slight expansion factor yields a volume of 631 Å^3 for monoolein as a whole at 25 °C.[6] Thus, the head group occupies 162 Å^3 using the old CRC handbook value for the density of monoolein; the same calculation using our new results yields a head group volume of 129 Å^3. Support for this dramatic difference can be found by considering monoacetin, which, chemically, is essentially monoolein's head group plus a terminal methyl. The density of monoacetin is 1.21 g cm^{-3}, as found in CRC-Handbook;[60] its volume minus that of the terminal methyl yields 128 Å^3, which is readily compatible with our results and in disagreement with the old literature values. Another item of support for our result can be found using ChemSpider, a freely available online chemical database owned by the Royal Society of Chemistry. Using ACD/Labs software, ChemSpider lists the predicted density of monoolein as 1.0 ± 0.1 g cm^{-3}, which is compatible with our result and in conflict with the older literature values.[61]

Also, our new results can resolve a puzzle in the literature by considering the electron density of the monoolein head group.

X-ray diffraction is sensitive to differences in electron densities. Phospholipids have head group electron densities of around 0.54 e Å^{-3} and water has an electron density of around 0.33 e Å^{-3}; consequently the phospholipid head group has prominent, well defined peaks in electron density reconstructions utilizing X-ray data. There is also good agreement between simple strip models and those reconstructions.[6] Using the old CRC handbook density results in an electron density of 0.39 e Å^{-3} for monoolein's headgroup, which suggests that electron density reconstructions of monoolein will not result in well defined head group peaks. Indeed, modeling based on this value results in reconstructions in which artifact peaks are larger than the head group peaks. However, reconstructions of actual monoolein X-ray data result in well defined head group peaks and no major artifact peaks. To summarize, the phosopholipid modeling and data matched well; the monoolein modeling and data did not match well.[6] Using our new measurements results in an electron density of 0.49 e Å^{-3} for monoolein's head group density. This is comparable to the density for phospholipid head groups, which in turn suggests that electron density reconstructions for monoolein should result in well defined headgroup peaks, which is indeed what is seen. We anticipate further exploring and exploiting this feature in future work.

3.3 DSC scans and kinetic phase diagram

Baseline corrected DSC scans are shown in Fig. 3 for monoolein in a 2 mol kg^{-1} solution of sucrose.

Enthalpies were quite small, of the order 1 mJ mg^{-1}, as is typical for these systems.[41] The enthalpies varied slightly with ramp rate and composition; the variations did not exhibit a discernible pattern. However, the locations and widths of the transitions were readily reproducible and yield useful results. As is generally the case, the phase transition location is shifted further as the temperature scan rate increases. An interesting feature of this system can readily be seen in that the cooling transitions are shifted much more than the heating transitions.

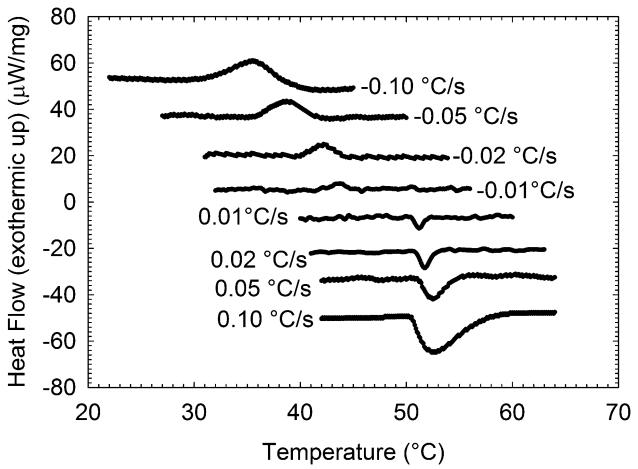

Fig. 3 DSC scans for monoolein in a 2 mol kg^{-1} sucrose solution. A linear baseline has been subtracted from each scan and they have been offset for visibility. On the bottom are the heating scans, with the temperature ramp rate of the scan to the left of the trace; on the top are shown the cooling scans, with the ramp rate to the right.

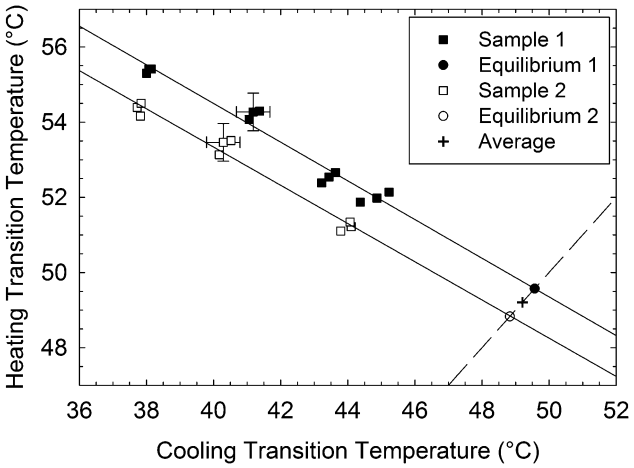

Fig. 4 Determination of the equilibrium phase transition value. For each sample, the heating transition temperature ($T_{heating}$) *vs.* the cooling transition temperature ($T_{cooling}$) was plotted and fit to a straight line, shown as a solid line for each sample. Each data point represents a pair of heating and cooling scans for a given sample; each sample was heated and cooled several times at each scan rate. The equilibrium transition temperature for each sample was determined to be the intersection of this fitted line with the equilibrium $T_{heating} = T_{cooling}$ line, shown as a dashed line. The equilibrium values for each sample were then averaged.

This asymmetry in the location of the cubic–H_{II} transition for monoolein and sucrose solutions is in marked contrast to the symmetry seen in the L_α–H_{II} phase transition observed in phospholipid and water systems.[22,62] The equilibrium phase transition temperature (T_0) can be found by plotting the phase transition temperature seen on heating ($T_{heating}$) *versus* the temperature seen on cooling ($T_{cooling}$) and extrapolating to the point where the two are equal. In practice, this is done by making a linear fit and determining where that fit intersects with the $T_{heating} = T_{cooling}$ line (see Fig. 4).[22,62]

The phase transition temperature dependence on temperature ramp rate and sucrose concentration can be summarized with a kinetic phase diagram (see Fig. 5).

Let us define the heating hysteresis as $\Delta T_{heating} = |T_{heating} - T_0|$ and the cooling hysteresis as $\Delta T_{cooling} = |T_{cooling} - T_0|$. A general feature is that the amount of hysteresis increases greatly with sucrose concentration. From the diagram, there is clear asymmetry in the heating and cooling hysteresis for lower sucrose concentrations but the asymmetry is reduced at higher concentrations. For both heating and cooling, the hysteresis markedly increases with sucrose concentration. The equilibrium phase transition temperature is strongly affected, being dropped by 19.8 °C (mol kg^{-1})$^{-1}$ of sucrose concentration. By comparison, the effect of sucrose on the cubic–H_{II} transition is typically twice as great as on the L_α–H_{II} transition.[42] Pleasingly, the extrapolated equilibrium phase transition temperature for pure water exactly matches the literature value of 90 °C.[1]

3.4 Transition width and FWHM

In addition to the location of the transition, one can also extract valuable information from the widths of the DSC scans. In keeping with previous kinetics work, the transition width τ is

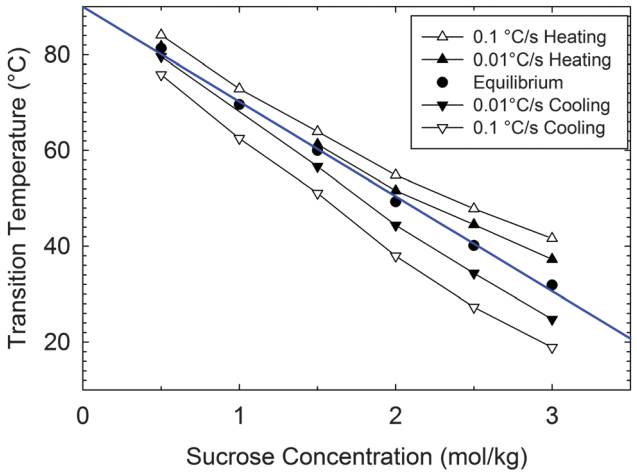

Fig. 5 Kinetic phase diagram for monoolein and sucrose solution mixtures. The measured heating and cooling phase transition temperatures are marked with upward and downward pointing triangles, respectively. Solid black lines connect points at the same temperature ramp rate and are there to guide the eye. The extrapolated equilibrium phase transition temperatures are depicted with filled circles and are fit to a straight line. The linear fit is shown as a solid blue line with an intercept of 90.0 °C and a slope of 19.8 °C (mol kg^{-1})$^{-1}$.

defined as the time for the phase transition to go from 1/4 to 3/4 completed.[22,62] However, for DSC data, it is commonplace to report the FWHM (full width, half maximum). These quantities can be straightforwardly related by the following calculation. Let us approximate the shape of the DSC trace as a Gaussian. Consequently, we define a dimensionless Gaussian that has been normalized so that the total area under the Gaussian is 1, namely

$$g(t) = \frac{1}{\sqrt{\pi}} e^{-t^2}. \quad (1)$$

The FWHM is then

$$\mathrm{FWHM} = 2\sqrt{\ln 2}. \quad (2)$$

In a region centered on the Gaussian, ranging from $-x$ to $+x$, the area under the Gaussian is given by the error function

$$\mathrm{Erf}(x) = \int_{-x}^{+x} g(t)\mathrm{d}t. \quad (3)$$

The normalization of the Gaussian can be economically stated as $\mathrm{Erf}(\infty) = 1$ and $\mathrm{Erf}(x)$ can be physically interpreted as the fraction of the phase transition that is completed in the interval from $-x$ to $+x$.

We can now find the transition width τ that corresponds to half the transition being completed. Mathematically, this is

$$\mathrm{Erf}(\tau/2) = 1/2, \quad (4)$$

which can be numerically solved to yield

$$\tau \approx 0.954. \quad (5)$$

Consequently, τ can be readily determined from the FWHM by

$$\tau \approx \frac{0.954}{2\sqrt{\ln 2}}\mathrm{FWHM} \approx 0.573\mathrm{FWHM}. \quad (6)$$

3.5 Hysteresis, width and Avrami analysis

The hysteresis is well fit by a power law (see Fig. 6) and so we can write

$$\Delta T_{\mathrm{cooling}} = |T_{\mathrm{cooling}} - T_0| = \alpha_C r^{\beta}, \quad (7)$$

where $\Delta T_{\mathrm{cooling}}$ is the cooling hysteresis, T_{cooling} is the phase transition temperature seen on cooling, T_0 is the equilibrium phase transition temperature, r is the cooling rate, and α_C and β are fit constants. The heating hysteresis is defined in a similar fashion and utilizes the same exponent β from the fit of the cooling data. The cooling widths also follow power law behavior (see Fig. 7) with the same exponent β, allowing us to state

$$\tau_C = \alpha_{\tau_C} r^{\beta}, \quad (8)$$

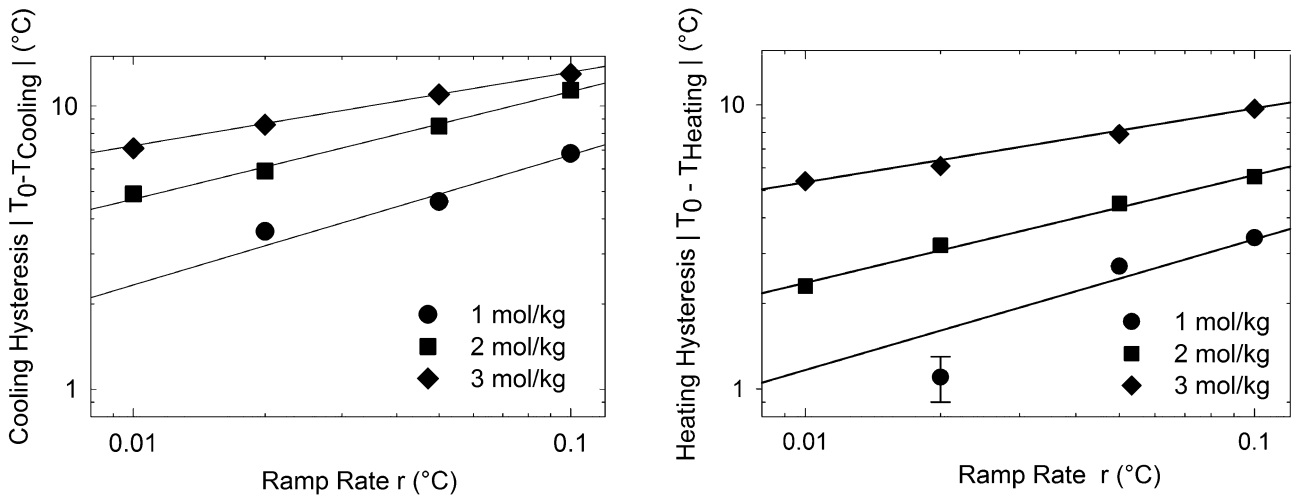

Fig. 6 Asymmetric hysteresis seen on heating and cooling. Error bars are of the order or smaller than the symbol sizes, except for one data point in which the error bars are explicitly shown. Power law fits to the data are shown as solid lines. Only integral sucrose concentrations are shown for clarity; a complete list of the power law fit results for all of the data can be found in Table 1.

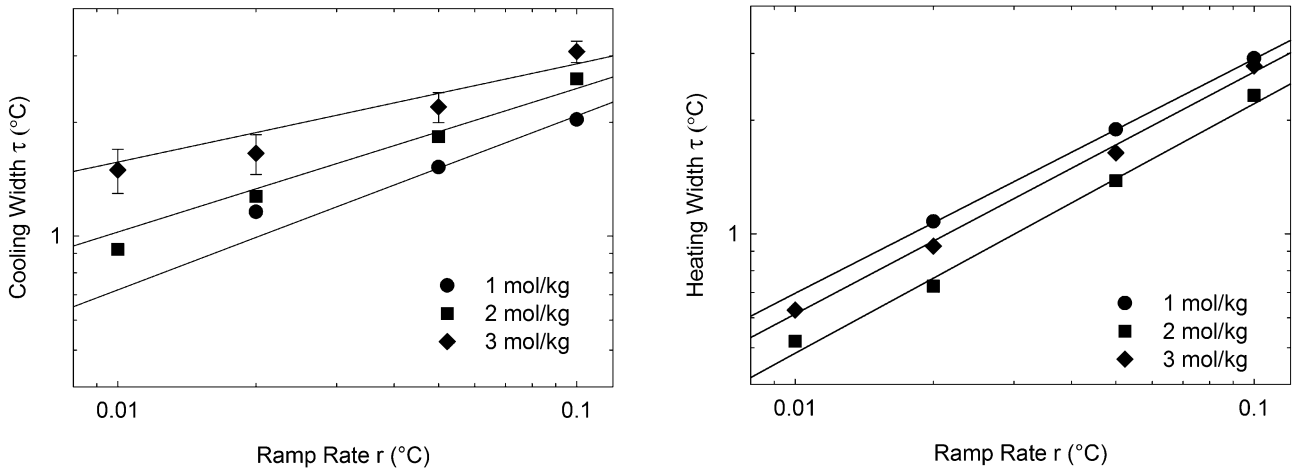

Fig. 7 Asymmetric cooling widths on heating and cooling. Representative error bars are shown for one set of data and power law fits to the data are shown as solid lines. Fits to the cooling widths used the same exponent found from fitting the heating hysteresis data; the fitted coefficients can be found in Table 1. Note that the heating widths are clustered about the same values and do not vary monotonically with sucrose concentration.

Table 1 Cooling and heating hysteresis parameters for monoolein in excess sucrose–water solutions. The cooling hysteresis, $\Delta T_{cooling} = |T_{cooling} - T_0|$, is given by $\alpha_C r^{\beta}$, where α_C and β are from the table and r is the ramp rate in °C s^{-1}. The heating hysteresis is given in the same manner. The width of the cooling transition, τ_C, is found by $\alpha_{\tau_c} r^{\beta}$. Avrami exponents for the cooling transition, n_C, are calculated and found to be roughly in the range of 2 to 2.5. The heating widths did not follow the same pattern and are treated in a separate table (see Table 2)

Hysteresis parameters, cooling widths and Avrami exponents					
Molality (mol kg^{-1})	α_C (°C/(°C s^{-1})$^{\beta}$)	α_H (°C/(°C s^{-1})$^{\beta}$)	β (unitless)	α_{τ_c} (°C/(°C s^{-1})$^{\beta}$)	n_C (unitless)
0.5	18.3	9.6	0.53	6.2	2.2
1.0	19.4	9.7	0.46	6.0	2.1
1.5	20.8	9.7	0.37	4.6	2.4
2.0	27.0	13.6	0.38	5.9	2.5
2.5	26.5	16.3	0.32	5.8	2.1
3.0	24.0	17.7	0.26	5.2	1.8

where τ_C is the width of the cooling transition and α_{τ_c} is a constant derived from a fit. A compilation of the fit constants can be found in Table 1.

For low sucrose concentrations, roughly twice the hysteresis is seen on cooling as opposed to heating; as sucrose concentration increases, this asymmetry is reduced (see Fig. 8). The exponent β, which governs both cooling and heating hysteresis and the width of the cooling hysteresis, decreases markedly with increasing sucrose concentration (see Fig. 8).

In this plot of β, there seems to be a possible shift at around 1.5 to 2 mol kg^{-1} sucrose concentration, which is where the cooling and heating asymmetry starts to be reduced. Interestingly, the heating widths don't exhibit much of a sucrose concentration dependence and are clustered around the same values. As the sucrose concentration increases, so does the viscosity of the solution. The increased viscosity could very well affect the lipid kinetics and may be responsible for the aforementioned shift.

With hysteresis and transition width data in hand, we can now proceed with an Avrami analysis by calculating the Avrami exponent. At the most fundamental level, the Avrami exponent tells how the amount of the new phase depends on time at the very start of the phase transition. In brief, if χ is the fraction of the system that is in the new phase, t is time and n is the Avrami exponent, then

$$\chi \sim t^n \text{ where } \chi \ll 1. \quad (9)$$

If the phase transition proceeds by nucleation and growth, one can connect the Avrami exponent to the dimensionality of the pathway of the phase transition and the nucleation rate by which the transition is initiated. If a transition proceeds from a fixed number of nucleation sites, the Avrami exponent matches the dimensionality of the phase transition pathway. To wit, if the new phase grows in a linear fashion from a nucleation site, the Avrami exponent is one; if the growth is planar, the Avrami exponent is two, *etc.* If instead there is a constant rate of spontaneous nucleation, the Avrami exponent is increased by one, so that linear growth results in an Avrami exponent of two, and so on. If the rate of nucleation increases over time, the Avrami exponent also rises. Basic Avrami theory deals with phase transitions initiated by a temperature jump (see Schultz[63] for the basics) and was extended to phase transitions driven by temperature ramps Ozawa.[64] For systems exhibiting power law behavior, it has been further refined and the following relation derived,[22]

$$n = (\alpha r^{\beta})\left(\frac{\beta}{\tau \ln 2}\right), \quad (10)$$

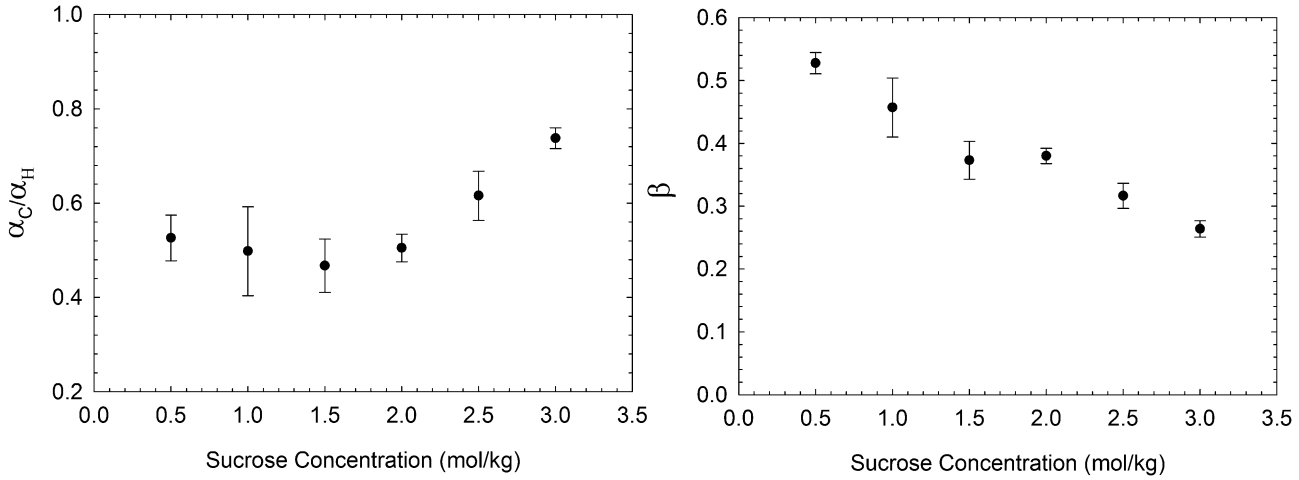

Fig. 8 Left: ratio of the coefficients of heating and cooling hysteresis fits plotted *vs.* sucrose concentration. Right: exponent from power law fit of cooling hysteresis data *vs.* sucrose concentration. Note that this same exponent was used to well fit the cooling hysteresis width data and the heating hysteresis data.

where n is the Avrami exponent and α, β, r and τ are as defined earlier.

When τ exhibits the same power law exponent as the hysteresis, as is the case on cooling, we can write $\tau_C = \alpha_{\tau_C} r^{\beta}$, and our expression for the Avrami exponent, n, simplifies to a ramp rate independent expression, namely,

$$n = \frac{\alpha_C \beta}{\alpha_{\tau_C} \ln 2} \tag{11}$$

A compilation of the ramp rate independent Avrami exponents seen on cooling can be found in Table 1. The exponents fall in the range from around 2 to 2.5. One possible interpretation is that the cooling transition propagates *via* a one dimensional process that has a nearly constant nucleation rate; another possible scenario is that the transition proceeds primarily from a fixed number of nucleation sites and propagates *via* a two dimensional process.

The situation on heating is a bit more complicated, as the Avrami exponent ranges from about 1 to 3 and depends on both ramp rate and sucrose concentration (see Table 2).

Table 2 Avrami exponents for the cubic to H_{II} heating transition in excess sucrose–water solutions. In contrast to the cooling transtion, there is a marked dependence on ramp rate and sucrose solution concentration, with the Avrami exponent rising with increasing sucrose concentration and decreasing ramp rate

Heating Avrami exponents (n_H)				
	Ramp rate (°C s^{-1})			
Molality (mol kg^{-1})	0.1	0.05	0.02	0.01
0.5	0.9	1.0	0.7	0.6
1.0	0.8	0.9	1.0	n/a
1.5	0.9	1.2	0.8	1.8
2.0	1.3	1.7	2.3	2.5
2.5	1.4	1.9	2.8	2.6
3.0	1.3	1.9	2.6	3.2

Two general trends can be observed; the Avrami exponent increases as the ramp rate is reduced and as the sucrose concentration is increased. There does appear to be a slight decrease in the Avrami exponent for slower ramp rates for the 0.5 mol kg^{-1} sucrose sample; however, the hysteresis is quite small at this low concentration and so these values have a high uncertainty. A possible interpretation of the general trends is that the transition proceeds by a one dimensional process that is initiated both by a fixed number of nucleation sites and spontaneous nucleation sites that appear at an increasing rate over time. In this scenario, transitions that happen quickly should be dominated by fixed nucleation sites and yield an Avrami exponent close to one; transitions that happen slowly would allow for greater contributions from spontaneous nucleation sites, resulting in a larger Avrami exponent. As both reducing the ramp rate and increasing the sucrose concentration result in an increase in the time the phase transition takes, this picture is consistent with the general trends we observe.

Besides classical nucleation and growth scenarios, it is also worth considering a non-classical picture. Because the cubic phase is so deeply perforated, it could very well be that the timing of the transition to this phase is dominated by pore formation; in this case, the cooling Avrami exponent reflects the time dependence of the pore formation. Likewise, the transition from the cubic phase to the H_{II} phase could be dominated by pore absorption or repair and that the heating Avrami exponents reflect this process.

3.6 Structure

It is important to consider the geometry of structures involved in the phase transition (see Fig. 1). Key parameters are the water weight fractions and lattice parameters for the cubic and H_{II} phases and the density of monoolein, which are summarized in Table 3.

For the following calculations, V_L is the volume of monoolein, ρ_L is the density of monoolein, ρ_w is the density of water,

Table 3 Structural properties of monoolein and excess water at the cubic–H_{II} phase transition temperature of 90 °C

Properties of monoolein in excess water at 90 °C	
Formula	$C_{21}H_{40}O_4$
Molar Mass	356.54 g mol^{-1}
Enthalpy[a] (cubic–H_{II})	0.3 kJ mol^{-1}
Volume of monoolein	619 Å^3
Density of monoolein	0.957 g cm^{-3}
Density of water	0.965 g cm^{-3}

Phases	Cubic	H_{II}
Lattice parameter[b]	70.5 Å	53.9 Å
Water weight fraction[b]	0.25	0.23
Waters per lipid	6.6	5.9
Average lipid length (l)	15.4 Å	14.8 Å
Average water radius (r_w)	12.5 Å	13.6 Å
Average head group area (A_L)	30.9 Å^2	27.2 Å^2

[a] Enthalpy is from Czeslik *et al.*[41] [b] Values from Briggs *et al.*[1] Average lipid length, water radius and head group area are all taken to be at the water–lipid (Luzzati) interface; calculations of these quantities are detailed in the text.

C_w is the water weight fraction, ϕ_w is the water volume fraction, a is the lattice parameter, l is the average lipid length, A_L is the area per lipid at the lipid–water (Luzzati) interface, and r_w is the average radius of the water channels. For the D-surface based cubic phase, we have the additional parameters σ and χ which are, respectively, the area of the minimal surface in a unit cell of unitary dimension and the Euler-Poincare characteristic and have the values 1.919 and −2. Formulas are taken from[3] and used with minor modification.

The volume fraction of water (ϕ_w) can be found *via*

$$\phi_w = \frac{C_w}{C_w + (1 - C_w)(\rho_w/\rho_L)} \quad (12)$$

where C_w is the water weight fraction, ρ_w is the density of water and ρ_L is the density of lipid. The densities are close enough that the water weight fractions and water volume fractions match to two significant figures.

In cubic phase, the monolayer thickness can be found by

$$1 - \phi_w = 2\sigma\left(\frac{l}{a}\right) + \frac{4}{3}\pi\chi\left(\frac{l}{a}\right)^3. \quad (13)$$

and the area per lipid is given by

$$A_L = 2V_L\frac{\sigma a^2 + 2\pi\chi l^2}{(1 - \phi_w)a^3}. \quad (14)$$

An estimate of the average radius of the water channels in the cubic phase is given by the following minimal surface based formula,

$$r_w = \left(-\frac{\sigma}{2\pi\chi}\right)^{1/2} a - l. \quad (15)$$

For the H_{II} phase, the radius of the water core is given by

$$r_w = \frac{1}{2}\sqrt{\left(\frac{2\sqrt{3}}{\pi}\right)\phi_w a^2} \quad (16)$$

The area per lipid can be calculated *via*

$$A_L = \frac{4\pi r_w V_l}{\sqrt{3}a^2(1 - \phi_w)} \quad (17)$$

The average lipid length requires a bit more consideration, as there is substantial variation of the length in the hexagonal phase. It has been shown that a volume weighted average[7] can be found to a high precision by

$$l = \left(\frac{1}{2}a - r_w\right)\left[1.1084 + 0.0572\left(\frac{r_w}{\frac{1}{2}a - r_w} - 1\right)\right]. \quad (18)$$

The results of all of these dimensional calculations are contained in Table 3. Using these results, we can see monoolein's length contracts by about 4% and the head group area decreases by 12% in the cubic–H_{II} transition.

As a comparison, one can consider the phase transition dimensions for *rac*-di-12:0 β-GlcDAG.[65] As expected, there is hysteresis and the phase diagrams seen on heating and cooling are different. The data in the paper is from the cooling diagram and the H_{II}–cubic transition is about 70 °C for *rac*-di-12:0 β-GlcDAG. At that point, the lipid length in the cubic phase is about 15.8 Å. In the H_{II} phase, r_w is 16.0 Å and $a/2 - r_w$ is about 13.5 Å, which results in an average lipid length of 15.1 Å. The average lipid length shrinks by about 5%. The area per volume, A_L/V_L, is 0.051 Å^{-1} in the cubic phase and 0.045 Å^{-1} in the H_{II} phase. As the volume change between fluid phases is a good deal less than 1%,[11] we will assume a roughly constant volume across the transition. This results in a reduction of the area by about 12%. Given that *rac*-di-12:0 β-GlcDAG is a lipid with two saturated tails 12 carbons long and that monoolein has a single monounsaturated tail that is 18 carbons long, the close correspondence of these changes is quite intriguing.

Another interesting comparison can be made to DOPE's (dioleoyl phosphatidylethanolamine) L_α–H_{II} transition. DOPE's two tails have the same structure as monoolein's single tail. During the transition, DOPE's length contracts by about 10% and the head group area decreases by about 22%.[7] Thermodynamically, the cubic phase is intermediate between the L_α and the H_{II} phase, which makes sense given that the structure has curvatures that vary from flat to highly curved. Consequently, it also makes sense that these changes in lipid length and head group area are intermediate, being about half of those seen in the L_α–H_{II} system. Now, there are substantial differences between these systems; they have different head groups, numbers of tails and the transitions are separated by almost 90 °C. The fact that these systems can none the less be sensibly correlated suggests that these structural changes might well be of deep and broadly applicable significance.

3.7 Thermodynamics

A useful relation of the Clausius–Clapeyron type that governs the shift of the phase transition temperature of a system under the influence of a bulk solution has been derived[42] and is

$$\frac{dT}{dc} = \frac{k_B T^2}{Q}\left[\Delta N_w - \frac{1}{c}\Delta N_c\right], \quad (19)$$

where T is the phase transition temperature, k_B is Boltzmann's constant, c is the bulk concentration of the solute, Q is the latent heat of the transition, ΔN_w is the change in the number water molecules going from the lower to the higher temperature phase and ΔN_c is likewise the change in the number of solute molecules. In our case, the solute is sucrose. It is also noted in passing that c is best expressed as a unitless mole ratio; so a c of 1 mole of sucrose per kg of water would be 1 mole of sucrose per 55.5 moles of water. Likewise, a proper normalization should be followed; we prefer to consider Q, ΔN_w and ΔN_c as per lipid quantities.

The quantity $\frac{1}{c}\Delta N_c$ is the change in the number of water molecules required to match the concentration in bulk; if the actual change in water molecules, ΔN_w, is different from this, that difference is the change in the number of excluding waters. These excluding waters are not available to hydrate the solute and so are part of the hydration shell. This can be simply written as

$$\Delta N_w^{ex} = \Delta N_w - \frac{1}{c}\Delta N_c, \tag{20}$$

where ΔN_w^{ex} is the change in the number of excluding waters. Combining these two equations and solving for the change in excluding waters yields

$$\Delta N_w^{ex} = \frac{dT}{dc}\left(\frac{Q}{k_B T^2}\right) = -0.3 \text{ waters per lipid} \tag{21}$$

This value does not tell us the number of excluding waters in phase; however, we can use it to evaluate the plausibility of a variety of scenarios. The simplest scenario to consider is that of no excluding water in either phase; this would result in a $\frac{dT}{dc} = 0$ and so this case can be ruled out. In scenario that the sucrose is entirely excluded in one phase and there are no excluding waters in the other phase, the magnitude of the change in the number of excluding waters would be equal to the waters per lipid in the phase in which sucrose is excluded. This is therefore likewise ruled out as the size of ΔN_w^{ex} would be off by over an order of magnitude. Next, one considers the case where all of the waters in phases are excluding waters; this results in a $\Delta N_w^{ex} = -0.7$, which is of the right magnitude, but still off by a factor of two. This possibility also seems remote given the relatively commodious size of the water channels compared to the dimensions of a sucrose molecule. A final possibility to consider is that there is a hydration shell of thickness t extending from each of the lipid head groups. By simple geometric approximation, we would expect

$$\Delta N_w^{ex} = \frac{(A_{hex} - A_{cubic})t}{V_w} \tag{22}$$

where A_{hex} and A_{cubic} are, respectively, the head group areas in the H_{II} phase and cubic phase and V_w is the volume of a water molecule, which is taken to be 30 Å^3. If the hydration shell is about 2.5 Å thick, of order of a single layer of water molecules, this would correspond to a $\Delta N_w^{ex} = -0.3$, which pleasingly matches our experimental result.

4 Conclusion

Sucrose has a powerful effect on the cubic–H_{II} phase transition of monoolein, dropping the phase transition temperature and greatly increasing the hysteresis. Control of the phase transition is a useful tool for monoolein's many uses, including drug delivery systems. Likewise, this study offers a useful base for further probing this transition. Control of the duration of the transition allows one to pick a time scale most favorable for the technique one wishes to use. Effects of other solutes can be examined to determine what effects are compound specific and which are more general features. A classical Avrami analysis suggests the heating cubic–H_{II} transition proceeds *via* a one dimensional pathway and that the cooling H_{II}–cubic transition occurs *via* a one or two dimensional pathway. A non-classical picture is that the transition is wholly dominated by pore formation and destruction, with the Avrami exponents revealing the time dependence of these processes. Future work could include detailed exploration of either of these pictures, as well as efforts to deconvolute temperature ramp rate data into an isothermal phase transition model.

Correct values for the temperature dependent density of monoolein are essential to properly understanding the structure of these phases; preliminary calculations indicate that this new data will have a profound effect on the electron densities used in modeling X-ray diffraction data. We also show that the lipid length decreases by about 4% and that the head group area decreases by 12%, changes that match closely with a dissimilar lipid (*rac*-di-12:0 β-GlcDAG) in the same transition. These changes are about half that seen in the L_α–H_{II} transition, which can be rationalized by recognizing the intermediate location of the cubic phase between the L_α and H_{II} phases. Structural work combined with thermodynamic insights suggests that there is a roughly one water layer thick hydration shell for monoolein. Much can be gained from thorough characterization of a system; besides contributing to a better understanding of monoolein's phase behavior, it is hoped that the reader has a renewed appreciation for fundamental quantities such as lipid volume and the value of a structural perspective based on these fundamental quantities.

Acknowledgements

Funding from Calvin College, Calvin College Alumni Association, the Howard Hughes Medical Institute, the Kuipers Applied Mathematics Endowment and the Michigan Space Grant Consortium is gratefully acknowledged. We thank Christopher Ver Hoef for preparation of the cubic phase illustration. Dr Harper is also thankful for IUPUI (Indiana University, Purdue University at Indianapolis) for hosting his sabbatical. Dr Tristram-Nagle acknowledges support from the National Institute of General Medical Sciences of the NIH under award GM44976.

References

1 J. Briggs, H. Chung and M. Caffrey, *J. Phys. II*, 1996, **6**, 723–751.
2 H. Qiu and M. Caffrey, *Biomaterials*, 2000, **21**, 223–234.

3 C. Kulkarni, W. Wachter, G. Iglesias-Salto, S. Engelskirchen and S. Ahualli, *Phys. Chem. Chem. Phys.*, 2011, **13**, 3004–3021.
4 A. Seddon, *Recent Developments in the Production, Analysis, and Applications of Cubic Phases Formed by Lipids*, Elsevier Academic Press Inc, San Diego, 2013, pp. 147–180.
5 P. Harper and S. Gruner, *Eur. Phys. J. E: Soft Matter Biol. Phys.*, 2000, **2**, 217–228.
6 P. Harper, S. Gruner, R. Lewis and R. McElhaney, *Eur. Phys. J. E: Soft Matter Biol. Phys.*, 2000, **2**, 229–245.
7 P. E. Harper, D. A. Mannock, R. N. A. H. Lewis, R. N. McElhaney and S. M. Gruner, *Biophys. J.*, 2001, **81**, 2693–2706.
8 M. Rappolt, A. Hickel, F. Bringezu and K. Lohner, *Biophys. J.*, 2003, **84**, 3111–3122.
9 M. Rappolt, A. Hodzic, B. Sartori, M. Ollivon and P. Laggner, *Chem. Phys. Lipids*, 2008, **154**, 46–55.
10 V. Kolev, A. Ivanova, G. Madjarova, A. Aserin and N. Garti, *J. Phys. Chem. B*, 2014, **118**, 5459–5470.
11 P. T. C. So, S. M. Gruner and S. Erramilli, *Phys. Rev. Lett.*, 1993, **70**, 3455.
12 R. N. Lewis, R. N. McElhaney, P. E. Harper, D. C. Turner and S. M. Gruner, *Biophys. J.*, 1994, **66**, 1088–1103.
13 D. Hajduk, P. Harper, S. Gruner, C. Honeker, G. Kim, E. Thomas and L. Fetters, *Macromolecules*, 1994, **27**, 4063–4075.
14 D. Hajduk, P. Harper, S. Gruner, C. Honeker, E. Thomas and L. Fetters, *Macromolecules*, 1995, **28**, 2570–2573.
15 P. I. Kuzmin, J. Zimmerberg, Y. A. Chizmadzhev and F. S. Cohen, *Proc. Natl. Acad. Sci. U. S. A.*, 2001, **98**, 7235–7240.
16 L. Yang and H. W. Huang, *Science*, 2002, **297**, 1877–1879.
17 L. V. Chernomordik, J. Zimmerberg and M. M. Kozlov, *J. Cell Biol.*, 2006, **175**, 201–207.
18 R. Willumeit, M. Kumpugdee, S. S. Funari, K. Lohner, B. P. Navas, K. Brandenburg, S. Linser and J. Andra, *Biochim. Biophys. Acta*, 2005, **1669**, 125–134.
19 H. Huang, *Biochim. Biophys. Acta, Biomembr.*, 2006, **1758**, 1292–1302.
20 A. Ramamoorthy, S. Thennarasu, D.-K. Lee, A. Tan and L. Maloy, *Biophys. J.*, 2006, **91**, 206–216.
21 A. Hickel, S. Danner-Pongratz, H. Amenitsch, G. Degovics, M. Rappolt, K. Lohner and G. Pabst, *Biochim. Biophys. Acta*, 2008, **1778**, 2325–2333.
22 P. L. Cook, J. L. Vanderhill, A. E. Cook, D. W. Van Norstrand, M. T. Gordon and P. E. Harper, *Chem. Phys. Lipids*, 2012, **165**, 270–276.
23 D. P. Siegel, *Biophys. J.*, 1999, **76**, 291–313.
24 J. Zimmerberg and M. Kozlov, *Nat. Rev. Mol. Cell Biol.*, 2006, **7**, 9–19.
25 D. Siegel, *Langmuir*, 2010, **26**, 8673–8683.
26 G. Shearman, O. Ces and R. Templer, *Soft Matter*, 2010, **6**, 256–262.
27 F. Campelo, C. Arnarez, S. Marrink and M. Kozlov, *Adv. Colloid Interface Sci.*, 2014, **208**, 25–33.
28 J. Shah, Y. Sadhale and D. Chilukuri, *Adv. Drug Delivery Rev.*, 2001, **47**, 229–250.
29 S. Rizwan, B. Boyd, T. Rades and S. Hook, *Expert Opin. Drug Delivery*, 2010, **7**, 1133–1144.
30 E. Nazaruk, M. Szlezak, E. Górecka, R. Bilewicz, Y. Osornio, P. Uebelhart and E. Landau, *Langmuir*, 2014, **30**, 1383–1390.
31 A. Mengesha, R. Wydra, J. Hilt and P. Bummer, *Pharm. Res.*, 2013, **30**, 3214–3224.
32 E. Landau and J. Rosenbusch, *Proc. Natl. Acad. Sci. U. S. A.*, 1996, **93**, 14532–14535.
33 V. Cherezov, D. Rosenbaum, M. Hanson, S. Rasmussen, F. Thian, T. Kobilka, H.-J. Choi, P. Kuhn, W. Weis, B. Kobilka and R. Stevens, *Science*, 2007, **318**, 1258–1265.
34 S. L. Keller, S. M. Bezrukov, S. M. Gruner, M. W. Tate, I. Vodyanoy and V. A. Parsegian, *Biophys. J.*, 1993, **65**, 23–27.
35 C. Kulkarni, A. Seddon, O. Ces and R. Templer, *Soft Matter*, 2010, **6**, 4339–4341.
36 C. Kulkarni, O. Ces, R. Templer and J. Seddon, *Soft Matter*, 2013, **9**, 6525–6531.
37 D. Gater, V. Réat, G. Czaplicki, O. Saurel, A. Milon, F. Jolibois and V. Cherezov, *Langmuir*, 2013, **29**, 8031–8038.
38 M. Caffrey, D. Li, N. Howe and S. Shah, *Philos. Trans. R. Soc., B*, 2014, **369**, 30621.
39 S. Abe and H. Takahashi, *Chem. Phys. Lipids*, 2007, **147**, 59–68.
40 F. Caboi, G. Amico, P. Pitzalis, M. Monduzzi, T. Nylander and K. Larsson, *Chem. Phys. Lipids*, 2001, **109**, 47–62.
41 C. Czeslik, R. Winter, G. Rapp and K. Bartels, *Biophys. J.*, 1995, **68**, 1423–1429.
42 R. Koynova, B. Tenchov and G. Rapp, *Biochim. Biophys. Acta*, 1997, **1326**, 167–170.
43 H. D. Andersen, C. Wang, L. Arleth, G. H. Peters and P. Westh, *Proc. Natl. Acad. Sci. U. S. A.*, 2011, **108**, 1874–1878.
44 P. Mariani, F. Rustichelli, L. Saturni and L. Cordone, *Eur. Biophys. J. Biophys. Lett.*, 1999, **28**, 294–301.
45 L. Saturni, F. Rustichelli, G. Di Gregorio, L. Cordone and P. Mariani, *Phys. Rev. E: Stat., Nonlinear, Soft Matter Phys.*, 2001, **64**, 040902.
46 Z. Wang, L. Zheng and T. Inoue, *J. Colloid Interface Sci.*, 2005, **288**, 638–641.
47 R. Mezzenga, M. Grigorov, Z. Zhang, C. Servais, L. Sagalowicz, A. Romoscanu, V. Khanna and C. Meyer, *Langmuir*, 2005, **21**, 6165–6169.
48 C. Conn, O. Ces, X. Mulet, S. Finet, R. Winter, J. Seddon and R. Templer, *Phys. Rev. Lett.*, 2006, **96**, 108102.
49 C. Conn, O. Ces, A. Squires, X. Mulet, R. Winter, S. Finet, R. Templer and J. Seddon, *Langmuir*, 2008, **24**, 2331–2340.
50 M. Rappolt, *Formation of Curved Membranes and Membrane Fusion Processes Studied by Synchrotron X-ray-Scattering Techniques*, 2013, vol. 17, pp. 29–54.
51 A. Squires, C. Conn, J. Seddon and R. Templer, *Soft Matter*, 2009, **5**, 4773–4779.
52 S. Jun, H. Zhang and J. Bechhoefer, *Phys. Rev. E: Stat., Nonlinear, Soft Matter Phys.*, 2005, **71**, 011908.
53 C. P. Yang and J. F. Nagle, *Phys. Rev. A: At., Mol., Opt. Phys.*, 1988, **37**, 3993.
54 K. M. Hallinen, S. Tristram-Nagle and J. F. Nagle, *Phys. Chem. Chem. Phys.*, 2012, **14**, 15452–15457.
55 J. Kraineva, R. Narayanan, E. Kondrashkina, P. Thiyagarajan and R. Winter, *Langmuir*, 2005, **21**, 3559–3571.

56 H. Vacklin, B. Khoo, K. Madan, J. Seddon and R. Templer, *Langmuir*, 2000, **16**, 4741–4748.
57 E. S. Lutton, *J. Am. Oil Chem. Soc.*, 1965, **42**, 1068–1070.
58 G. Lindblom, K. Larsson, L. Johansson, K. Fontell and S. Forsen, *J. Am. Chem. Soc.*, 1979, **101**, 5465–5470.
59 S. T. Hyde, S. Andersson, B. Ericsson and K. Larsson, *Z. Kristallogr.*, 1984, **168**, 213–219.
60 CRC-Handbook, *CRC Handbook of Chemistry and Physics*, CRC Press, Taylor & Francis Group, Boca Raton, Florida, 2005.
61 ChemSpider, ChemSpider results for monoolein, http://www.chemspider.com/Chemical-Structure.4446588.html, 2014, accessed: 2014-12-01.
62 G. E. S. Toombes, A. C. Finnefrock, M. W. Tate and S. M. Gruner, *Biophys. J.*, 2002, **82**, 2504–2510.
63 J. M. Schultz, *Polymer Crystallization*, Oxford University Press, New York, 2001.
64 T. Ozawa, *Polymer*, 1971, **12**, 150–158.
65 D. C. Turner, Z.-G. Wang, S. M. Gruner, D. A. Mannock and R. N. McElhaney, *J. Phys. II*, 1992, **2**, 2039–2063.

